Open Access Online Journal on Astronomy and Astrophysics

Acta Astrophysica Taurica

www.astrophysicatauricum.org

Acta Astrophys. Tau. 1(1) 6–12 (2020) doi:10.31059/aat.vol1.iss1.pp6-12

Dynamic processes in an active region in the initial and impulsive phases of the eruptive flare event on June 7, 2011

A.N. Babin, A.N. Koval

Crimean Astrophysical Observatory, Nauchny 298409, Crimea
e-mail: babin@craocrimea.ru

Submitted on March 7, 2019

ABSTRACT

We present the results of an analysis of H_α monochromatic and spectral observations obtained at the Crimean Astrophysical Observatory for an impressive filament eruption during a flare occurred on June 7, 2011. Our ground-based observations are combined with data acquired by multiple instruments onboard the Solar Dynamics Observatory (SDO/AIA, SDO/HMI). The evolution and dynamics of the eruptive process, the cause of eruption, the structure of the line-of-sight velocity field and fine internal structure of the eruptive filament are studied and a number of physical parameters of the eruptive filament are determined.

The results of the analysis have shown that: 1) The evolution of the filament eruption consists of two phases: the slow-rise phase, which began about two hours before the flare onset, and the fast-rise phase, which began almost simultaneously with the flare onset. 2) The eruptive filament had a very complex internal structure and complicated line-of-sight velocity field. The filament does not erupt as a single structure. Several discrete massive absorption fragments are seen with a large number of fine-structure elements inside fragments with different velocities, as well as many plasma blobs that detach from the fragments. 3) The motion of the filament fragments is a combination of rotational motion around the axis of the fragment and a movement as a whole towards the observer. The velocities of such plasma motions are determined. 4) H_α line profiles show a large variety of contrast values, Doppler half-widths and Doppler shifts in eruptive filament elements.

Key words: Sun, solar activity, eruptive filaments and flares

1 Introduction

Flare observations obtained with Skylab (1973–1974) have shown that they may be distinguished into two classes differed by the global magnetic field shapes in which they occur (Pallavichini et al., 1977). In some cases flares emerge in the system of loops that remain close throughout the whole phenomenon. In other cases magnetic lines of force become open, and the magnetic field and matter are ejected into the corona and interplanetary space by the eruptive filament and coronal mass ejections (KME). The first class of flares was named compact and the second one – eruptive. The term "eruptive flares" involves both two-ribbon flares and the eruption of filaments and other coronal configurations (Svestka and Cliver, 1992). The mechanisms that cause the ejection of matter and magnetic field from the solar atmosphere into the interplanetary space remain unresolved. A study of dynamics and structure of eruptive phenomena is required to determine physical processes causing the eruption.

The data on the dynamic phenomena in eruptive flares have been derived from observations with filters and are often constrained by an exploration of motions in the plate plane (Webb et al., 1976; McAllister et al., 1992, 1996; Khan et al., 1998). Spectral observations that allow the line-of-sight velocities to be derived are sparse (Kubota et al., 1992; Plunkett et al., 2000; Morimoto and Kurokawa, 2003). In order to establish a mechanism of solar eruptions, the initial stage of eruption should be explored, since observations show the flare activity to start some time before the beginning of the flare impulsive phase (Martin and Ramsey, 1972; Rust, 1976; De Jager and Svestka, 1985; Kahler et al., 1988). As stated above (Martin, 1989), the accuracy of describing a picture of matter motions and consequently the physical interpretation are strongly dependent on the quality of observations, i.e. on the fine structure resolution.

In this paper we study a complex eruptive flare event on June 7, 2011 occurred in the active region (AR) NOAA 11226, coordinates S20W55. We study the evolution and dynamics of the eruptive flare process, explore the filament structure, peculiarities of the line-of-sight velocity fields and physical conditions in the eruptive filament in the initial and impulsive phases of the flare through the analysis of high-quality spectral H_α-observations obtained with the 53 cm coronagraph KG-2 of the Crimean Astrophysical Observatory combined with monochromatic H_α-observations with the coronagraph KG-1 and observational data from

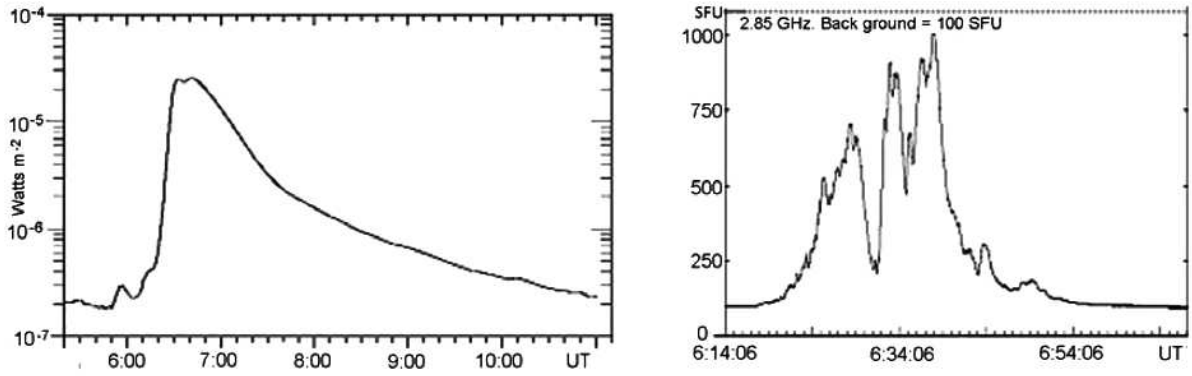

Fig. 1. Left: variation with time of the SXR flux in a band of 1–8 Å 07.06.2011 (1-minute data from GOES-15). Right: variation of microwave radio emission at a frequency of 2.85 GHz during the flare (Katsiveli, CrAO)

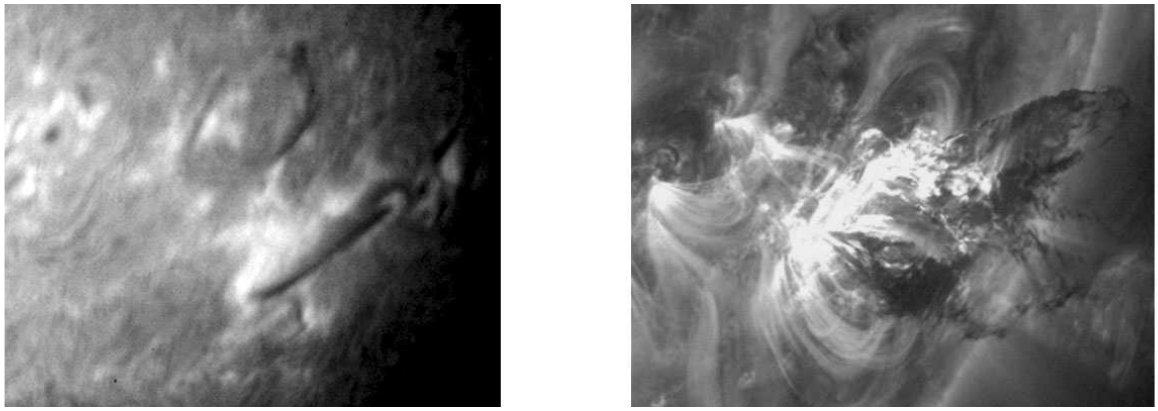

Fig. 2. Left: an H_α-image of the filament in the AR 11226 at 5:49:48 UT from observations with KG-1. Right: flare and filament eruption at 06:30 UT in a band of 171 Å based on data from SDO/AIA

the Solar Dynamics Observatory (SDO) (Lemen et al., 2012; Scherrer et al., 2012).

2 Observations and analysis

2.1 Event characteristics

According to the GOES observations, a flare of class 2N/M2.5, started at 06:16 UT, achieved its maximum at 06:41 UT and lasted about an hour and a half. A variation with time of the X-ray radiation in a band of 1–8 Å (GOES-15) and microwave radio emission at a frequency of 2.85 GHz (Katsiveli, CrAO) is presented in Fig. 1. The flare was two-ribbon accompanied by the filament eruption with ejection of a number of chromosphere matter into the corona, and it was a source of rapid coronal mass ejection (with a velocity of about 1250 km/s), as well as the post-flare strengthening of the gamma-ray flux. A striking example of the filament eruption in this event was observed with instruments mounted onboard SDO. Based on these observations, a series of works were carried out investigating various aspects of this eruptive event (Innes et al., 2012; Williams et al., 2013; Gilbert et al., 2013; Solov'ev, 2012; Li et al., 2012; Inglis and Gilbert, 2013; Cheng et al., 2012; van Driel-Gesztelyi et al, 2014; Carlyle J. et al., 2014; Yardley et al., 2016; Fainshtein et al., 2017). An H_α-image of the filament (from observations with KG-1), as well as flares and filament eruptions in a band of 171 Å (based on data from SDO/AIA) are presented in Fig. 2.

2.2 Magnetic field dynamics: morphology and evolution

The active region 11226 was a western component of the active complex comprised of three closely spaced sunspot groups. An image of the AR in the continuum, a magnetogram and filtergram in a band of 304 Å are shown in Fig. 3. The magnetic situation in the active region noticeably changed during its passing across the solar disk. Based on observations of sunspot magnetic fields at CrAO, in the immediate vicinity of sunspots of the predominating N-polarity, pores of both N- and S-polarity emerged and disappeared, sometimes with the formation of short-term delta-configurations of the magnetic field, what points to the complexity of the outward magnetic flux. Evolution of the magnetic field in the active complex and its effect on the evolution of the eruptive process are explored in detail by (Yardley et al., 2016). The dynamics of photospheric magnetic fields during the flare is presented by (Fainshtein et al., 2017) from measurements of the magnetic field vector by SDO/HMI. Since June 5 the AR was at the decomposition

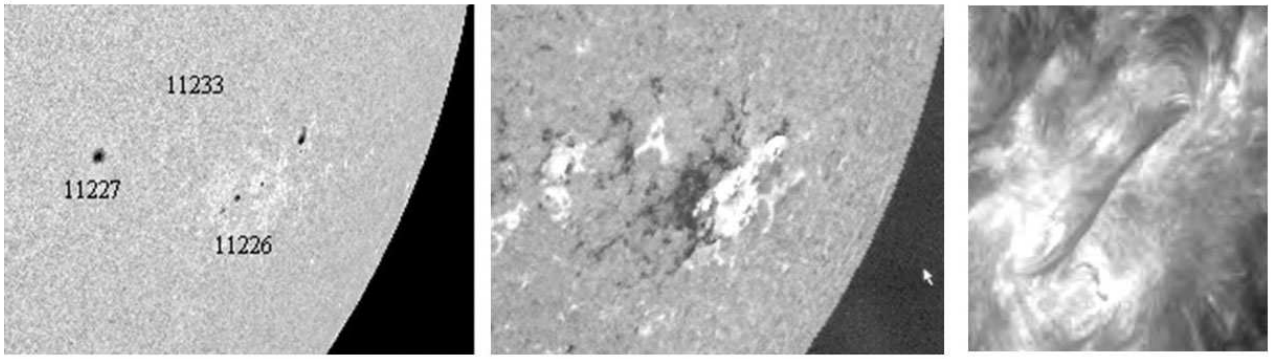

Fig. 3. Left and center: an image of the active complex in the continuum and a magnetogram of the longitudinal magnetic field (SDO/HMI). Right: an image of the AR 11226 in a band of 304Å HeII (SDO/AIA) on 07.06.2011 at 04:00 UT

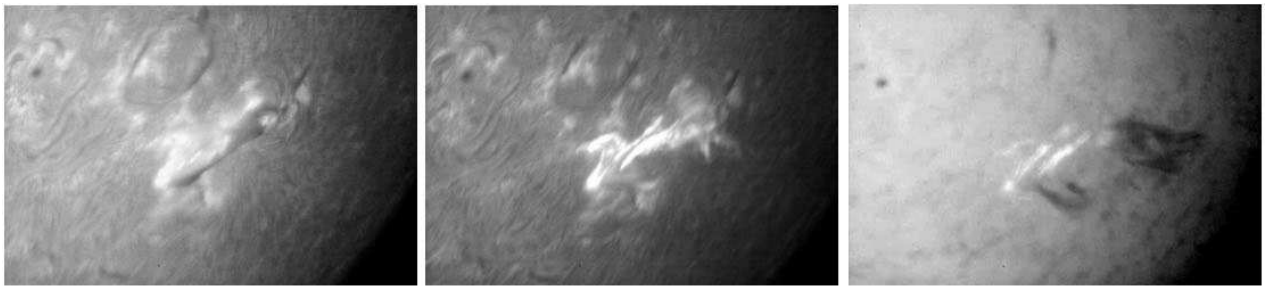

Fig. 4. Left and center: an image of the AR 11226 in the center of the H_α line at 06:12:39 and 06:23:42 UT, respectively. Right: an image in the blue wing of the H_α line at 06:26:14 UT (KG-1)

stage of basic sunspots, but the emersion of the new magnetic flux occurred directly during the flare as well. This is proved by the emergence of bright moustaches in the region of flare ribbons (Koval', 1965; Bruzek, 1967).

2.3 Evolution of the eruptive process

We analyze the evolution of the eruptive process based on EUV-images derived with SDO/AIA and monochromatic H_α-observations taken with the telescope KG-1 at CrAO. Fig. 4 demonstrates the H_α-image of the AR on June 7 several minutes before the eruption onset. The powerful filament located roughly in the NS direction along the polarity separating line roots by its ends close to the opposite polarity sunspots. The first indication of instability in the AR was a slow motion of the filament in the plate plane in the western direction (rise) that had started about 2 hours before the flare. The average motion rate of the filament central part in the plate plane during a period of 04:30–06:15 UT increased from 0.8 km/s to 1.9 km/s. At the same time, the filament morphology changed and the new absorbing structures appeared near the places of rooting by the filament into the photosphere. A slow motion of the filament was accompanied by the emergence of bright fine-structure non-stationary formations in the region of plage emission along the filament from east and microflares near the places of rooting by the filament. A slow rise of the filament passed on to the eruption stage at about 06:16–06:19 UT. The value of the motion rate of the filament central part at 06:17:42 UT achieved 25 km/s, and at 06:21:30 UT – 120 km/s. During the period of filament's passing into the eruption stage, a bright emission strip, rimming the filament, started to form and it had formed by 06:19 UT. The emission strip moved ahead of the filament along with it in the western direction. An interesting phenomenon is the emission dynamic ejection from the region of rooting of the filament's northern end, whose leading front extended in the plate plane in the western direction with a maximum rate of 575 km/s. The ejection was seen both in EUV and in H_α-radiation. A change of filament motion from slow to eruptive one coincides with the flare onset, which started from the emergence of compact formations on the place of the future eastern ribbon. Fig. 4 shows an image of the AR in the center of the H_α line at the beginning of the impulsive phase at 06:23:42 UT. Two flare ribbons are seen in it. The eastern ribbon closely follows the position of the bright flocculus to the east from the filament, and the western one – to the position at 06:12 UT.

2.4 Filament macrostructure: H_α monochromatic observations

The filtergram shows no filament in the center of the H_α line at 06:23:42 UT (Fig. 4). Here the eruptive process is well seen in the blue wing of the H_α line at 06:26:14 UT: the eruptive dark structures are seen on the filament ends, as if during the rise of the filament there occurred a rupture in its central part, and both ends remained rooted into the photosphere. A loop-like structure was formed on the southern end. A rise of

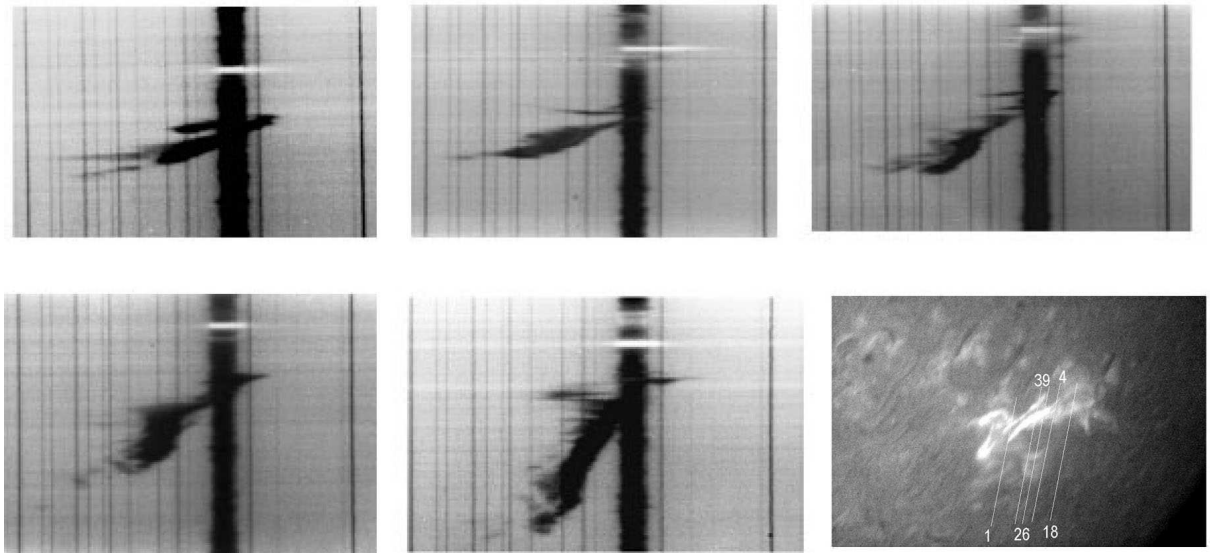

Fig. 5. Examples of H_α-spectra 1, 4, 18 (upper row) and 26, 39 (lower row) derived during a period of 06:26:30–06:31:09 UT at various positions of the spectrograph slit in the active region. The slit positions are marked by linear segments with numbers on the bottom right panel which shows the H_α-image of the AR at 06:23:42 UT. All images are in the positive mode

several well-resolved, variously oriented rope-like structures originates on the northern end. The rope-like structures intersect each other what points to variations in the direction of structures with height. These observations show the filament to consist of several individual twisted ropes, which during the eruption onset untwisted and rose at various angles to the solar surface. The fact that two different types of structures were observed on the filament ends states the filament microstructure to be various at different sites. The untwisting and detaching of filaments during the eruption into individual structures have been observed before by (Martres et al., 1980; Raadu et al., 1987; Vršnak, 1990; Uddin et al., 2004; Panasenko et al., 2013; Su and van Ballegooijen, 2013).

2.5 Line-of-sight velocity field and inner structure of the eruptive filament. Spectral observations

Spectral observations of the June 7, 2011 eruptive event have been derived at CrAO with the 52 cm coronagraph designed by G.M. Nikolskiy – A.A. Sazanov (KG-2). A flare spectrum was visually seen with KG-2 at 06:20 UT. During this time a two-ribbon structure had already formed in the Hα-flare. Large formations in absorption with high Doppler shifts were also seen in the spectrum. The photographic spectral observations started at 06:26:30 UT. We recorded a spectrum region of 6550–6575 Å, dispersion 0.578 Å/mm, exposure 0.15 s, an interval between frames of 3–5 s, a size of the solar image at the spectrograph slit of 180 mm. The quality of images made it possible to derive a spatial resolution of 1 arcsecond in the best frames. To extensively study the structure of the line-of-sight field during the eruption, H_α-spectrograms were taken at different positions of the spectrograph slit in the active region. Simultaneously with spectra, a solar image was recorded at the spectrograph slit through the H_α-filter.

We study H_α-spectra derived during a period of 06:26:30–06:34:30 UT that corresponds to the first and second sub-outbursts of the microwave radio emission and the rise to the maximum of the soft X-ray emission. The typical examples of H_α-spectra derived at various positions of the spectrograph slit in different time periods, and the position of the slit in the active region are presented in Fig. 5. No eruptive matter of the filament is seen in the H_α-images of the Sun at the spectrograph slit by reason of the exit from the bandpass of the H_α-filter due to the high Doppler velocities.

As seen in Fig. 5, in the eruptive filament by its spectrum it is possible to distinguish several types of motions observed at various parts of the eruption. The ejections are composed of several formations: basic high-density mass with lower Doppler shifts and ejections of less density with high line-of-sight velocities, which to a greater or a lesser extent are present in all the ejected fragments of the filament. The fragment's body is highly structured: inside the fragment there are structures having various intensities and Doppler shifts. While moving, the fragment retains its shape which is obviously supported by the elongated macrostructure of the magnetic field. In all spectra the main body of the ejected fragment is merged by a fine filament with the photosphere. The Doppler shift of the fragment increases along the slit with increasing distance from the place of rooting into the photosphere. A systematic variation of the Doppler shift along the slit causes the formation of structures inclined to dispersion, which are well seen in spectra derived at various slit positions. As the inclined structure is shifted in respect to the unshifted H_α line, then the observed picture may be interpreted as evidence for the plasma rotation of the filament fragment around its central axis during the motion as a whole. The rotational motions in prominences and filaments have extensively been studied before by (Rompolt, 1975; Ohman, 1969; Kurokawa et al., 1987; Plunkett et al., 2000), as well as in recent works by (Panasenko et al., 2013; Su and van Ballegooijen, 2013).

For several filament fragments and fine-structure elements, a detailed photometric analysis of spectra was per-

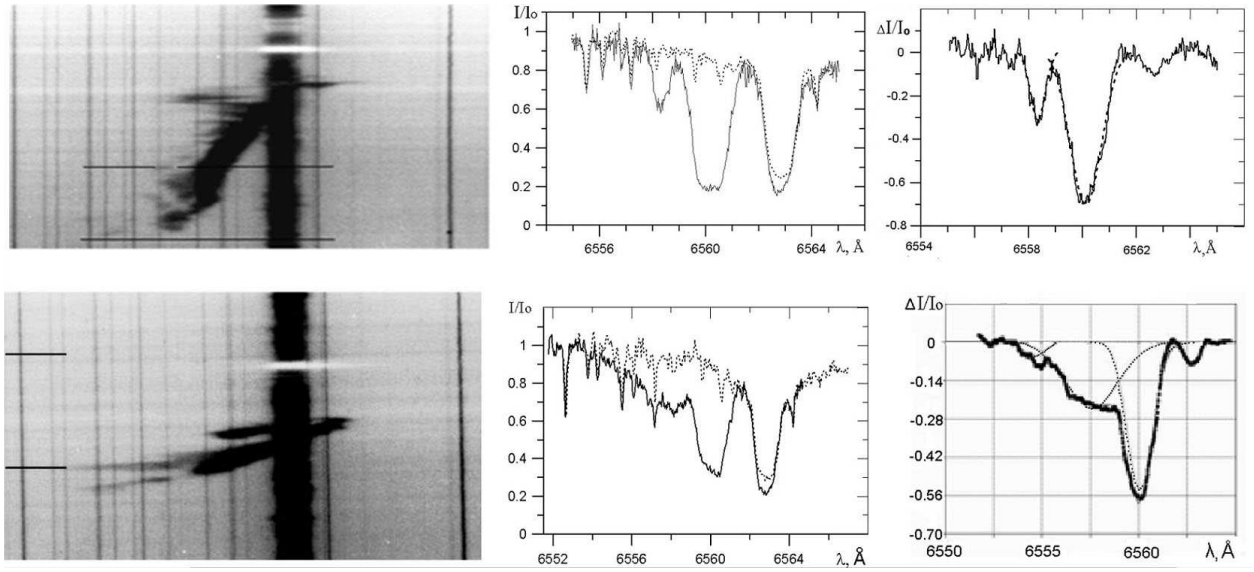

Fig. 6. Left: spectrograms of eruption. Center: photometric records of the filament fragments (solid line) and the undisturbed photosphere (dotted line) in regions marked in spectrograms. Right: contrast profiles of eruption and their approximations by Gaussians for the spectrum 1 (bottom) and spectrum 39 (top)

Table 1. Characteristics of H_α-profiles of two fragments of the eruptive filament

Time, UT	No. spectrum	Contrast $\Delta I/I_0$	Doppler half-width, Å	Doppler shift, Å
06:26:30	Sp. 1, r. 1	−0.53	0.660	−2.68
	r. 2	−0.25	1.466	−5.11
	r. 3	−0.05	0.494	−8.21
06:31:09	Sp. 39, r. 1	−0.77	0.560	−2.17
	r. 2	−0.34	0.275	−4.48

Table 2. Rotation rates of filament fragments V_r and motion as a whole V_f

No. spectrum	Time, UT	V_f, km/s	V_r, km/s
1	06:26:30	−40	126
4	06:27:05	−150	108
18	06:29:10	−154	75
39	06:31:09	−114	78

formed and contrast profiles of the H_α line in eruption were constructed. Fig. 6 shows microphotometric records along the dispersion of two filament fragments and the undisturbed H_α line profile, as well as contrast profiles. The absorption profiles are interpreted as absorption of solar radiation by a cloud of the emerged filament. Contrast profiles are taken by subtracting residual intensities of the nearby undisturbed photosphere contour from the residual intensities of the H_α line contour in eruption. From the analysis of the H_α-profiles in eruption, the values of contrast, Doppler half-widths and line-of-sight velocities of absorbing elements have been detected. Photometric sections of fragments along the dispersion exhibit that in most cases H_α-contours are complex: in the same region of the fragment at the spectrograph slit there are several discrete absorbing structures having various contrast, Doppler half-width, and line-of-sight velocity. In some cases (Fig. 6, spectrum 39) their contours are separated due to a great difference in the line-of-sight velocities, and element contours are well presented by Gaussians. In other cases (Fig. 6, spectrum 1) there is an overlap of individual structures' contours, and the resulting H_α profile proves to be highly complex. For instance, the contrast profile in Fig. 6, spectrum 1 is well shown by the overlapping of three Gaussians with different parameters, corresponding to three absorption elements. Table 1 exemplarily lists characteristics of H_α-profiles in two different fragments of the eruptive filament: contrast, Doppler width, and Doppler shift.

Measurements have shown that the line-of-sight velocities of the fine-structure elements lie between 150 km/s and 400 km/s. The sizes of elements are perpendicular to the dispersion direction – between 1.4 and 3 arcseconds. There is a large spread in Doppler half-widths and Doppler shifts depending on the slit position and eruption phase. Note that the contrast value is very high in large filament fragments.

For the inclined structures, in the spectrum of fragments, the measured by the Doppler shift velocity V_d may be reproduced as a sum of the rotation rate V_r and the fragment

motion rate as a whole V_f. Applying a method reported in (Plunkett et al., 2000), we detected rotation rates of fragments and their motion rates as a whole. The derived values for several fragments are listed in Table 2. The negative rates correspond to the Doppler shift in the blue region of the spectrum (a rise and motion towards the observer)

3 Results and discussion

On the basis of the analysis of H_α monochromatic and spectral observations, as well as data from SDO, we studied an early evolutionary stage of the eruptive flare event on June 7, 2011, explored a fine structure of the eruptive filament and inner motions along the line-of-sight, and analyzed the H_α line profiles in the eruptive filament during the flare impulsive phase. Results of the analysis show:

1. An eruptive event occurred in the active region which was at the stage of decay of main sunspots, however, the new magnetic flux was emerging. The magnetic field rearrangement, namely a variation of the sunspot structure and motions of the newly formed umbra fragments, disappearance of some magnetic flux, as well as emergence of the new magnetic flux in the immediate vicinity from the filament could cause an eruption. This confirms the results obtained before (see Webb et al., 1994; Yardley et al., 2016). Note that an emergence of the new magnetic flux was observed during the flare, too.
2. Evolution of the June 7, 2011 eruptive event is consistent with a two-phase picture of evolution of the eruptive filaments studied before, namely the existence of slow- and fast-rise phases (Moore and Roumeliotis, 1991; Sterling and Moore, 2005; Fainshtein et al., 2017). The strengthening of the filament slow motion was accompanied by a variation of its structure and emergence of the short-term fine-structure emission along the filament and near the regions of its rooting into the photosphere. The short-term brightenings at various wavelengths of electromagnetic radiation from radio to SXR before the flare onset were previously reported by (Schmahl et al., 1989; Chifor et al., 2007).
3. The flare started almost simultaneously with a passage of the filament into the eruption stage and with an eruption of high-speed bright matter in the plate plane at EUV wavelengths.
4. Observations with H_α-filter at the eruption onset have shown that the filament consists of several twisted ropes which during the eruption untwisted and rose at various angles to the solar surface. The twisting of macrostructures was different in various regions of the filament.
5. Spectral observations have shown that the line-of-sight velocity field in the filament is very complex and fine-structure. Eruptions are composed of the ejection of high-density (a contrast of up to −0.80) large filament fragments with a number of fine-structure elements inside the fragment and a flow of individual blobs with various densities and line-of-sight velocities, which are detached from the fragment. Line-of-sight velocities of blobs lie in the range from −150 km/s to −400 km/s.
6. The motion of large filament fragments may be exhibited by a combination of the rotation motion of the fragment around the filament central axis and motion as a whole directed towards the observer. The measured fragment rotation rates lie in the range from 75 km/s to 130 km/s, and motion rates as a whole are from −40 km/s to −150 km/s.
7. When moving, the fragment retains its shape with time, which is obviously supported by the elongated magnetic lines of force that remain associated with the photosphere in the initial period of eruption.
8. A characteristic feature of the eruption is the strong plasma inhomogeneity in all ejected fragments. The absorption is concentrated in discrete formations with a size of 1.4–3 arcseconds. H_α-profiles of individual structures are well represented by Gaussians having various intensities, Doppler widths, and Doppler shifts. This points to the difference in physical conditions under which blobs accelerated during the eruption. A more detailed study of the structure of ejections and the determination of physical parameters may be a target for further investigations.

4 Conclusions

If we consider our findings from the point of view of basic eruption models previously proposed in a series of works (see a discussion in Chifor et al., 2007), then the results of our observations mostly correspond to peculiarities predicted by the internal tether-cutting model. The true picture of motions and physical conditions in eruptive filaments may be obtained only with taking into account spectral observations whose quality allows us to resolve a fine structure of an order of 1 arcsec. The magnetic fields are very structured and complex, and this should be taken into account while constructing the eruption models. As the activation of a filament begins prior to the flare onset, this fact may be used as a short-term predictor of an eruption.

Authors are grateful to observers at the coronagraph KG-1 A.N. Shakhovskaya and T.M. Strelnik for providing with H_α monochromatic observations of the eruptive event, as well as to groups of researchers at SDO/AIA and SDO/HMI for the possibility of working with data. The research was partially supported with grants of the Russian Foundation for Basic Research No. 16-02-00221A and the Program of the RAS Presidium No. 28.

References

Koval' A.N., 1965. Izv. Krymsk. Astrofiz. Observ., vol. 33, p. 138. (In Russ.)
Bruzek A., 1967. Solar Phys., vol. 2, p. 451.
Carlyle J., Williams D.R., van Driel-Gesztelyi L., et al., 2014. Astrophys. J., vol. 788, p. 25.
Cheng X., Zhang J., Olmedo O., et al., 2012. Astrophys. J., vol. 745, p. L5.
Chifor C., Tripathi D., Mason H.E., and Dennis B.R., 2007. Astron. Astrophys, vol. 472, p. 967.
De Jager C. and Svestka Z., 1985. Solar Phys., vol. 100, p. 435.
Fainshtein V.G., Egorov Y.I., and Rudenko G.V., 2017. Geomagnetism and Aeronomy, vol. 57, no. 7, p. 906.
Gilbert H.R., Inglis A.R., Mays M.L., et al., 2013. Astrophys. J. Lett., vol. 776, p. L12.

Inglis A.R. and Gilbert H.R., 2013. Astrophys. J., vol. 777, p. 30.
Innes D.E., Cameron, R.H., Fletcher L., et al., 2012. Astron. Astrophys., vol. 540, p. L10.
Kahler S.W., Moore R.L., Kane S.R. and Zirin H., 1988. Astrophys. J., vol. 328, pp. 824–829.
Khan J.I., Uchida Y., McAllister A.H., et al., 1998. Astron. Astrophys., vol. 336, p. 753.
Kubota J., Kitai R., Tohmura I., and Uesugi A., 1992. Solar Phys., vol. 139, p. 65.
Kurokawa H., Hanaoka Y., Shibata K., and Uchida Y., 1987. Solar Phys., vol. 108, p. 257.
Lemen J.R., Title R., Akin D.J., et al., 2012. Solar Phys., vol. 275, p. 17.
Li T., Zhang Y., Yang S., and Liu V., 2012. Astrophys. J., vol. 746, p. L103.
Martin S.F., 1989. Solar Phys., vol. 121, no. 1/2, p. 215.
Martin S.F. and Ramsey H.E., 1972. in McIntosh P.S. and Dryer M. (Eds), Solar Activity Observation and Prediction, p. 371.
Martres M., Mouradian Z., and Soru-Escaunt I., 1980. in Moriyama F. and Henoux J.C. (Eds), Proceedings of the Japan-France Seminar on Solar Physics, p. 188.
McAllister A.H., Kurokawa H., Shibata K., Nitta N., 1996. Solar Phys., vol. 169, p. 123.
McAllister A.H., Uchida Y., Tsuneta S., Strong K.T., 1992. Publ. Astron. Soc. Japan, vol. 44, p. L205.
Moore R.L. and Roumeliotis G., 1991. in Svestka Z., et al. (Eds), Proceedings of Colloquium No. 133 of IAU, Eruptive Solar Flares, Springer-Verlag Berlin Heidelberg, vol. 399, p. 69.
Morimoto T. and Kurokawa H., 2003. Publ. Astron. Soc. Japan, vol. 55, p. 518.
Ohman Y., 1969. Solar Phys., vol. 9, p. 427.
Pallavichini R., Serio S., and Vaiana G.S., 1977. Astrophys. J., vol. 216, p. 108.
Panasenko O., Martin S.F., Velli M., and Vourlidas A., 2013. Solar Phys., vol. 287, p. 391.
Plunkett S.P., Vourlidas A., Simberova S., et al., 2000. Solar Phys., vol. 194, p. 371.
Raadu V.A., Malherbe J.M., Schmieder B. and Mein N., 1987. Solar Phys., vol. 109, p. 59.
Rompolt B., 1975. Solar Phys., vol. 41, p. 329.
Rust D.M., 1976. Solar Phys., vol. 47, p. 21.
Scherrer P.H., Schou J., Bush R.I., et al., 2012. Solar Phys., vol. 275, p. 229.
Schmahl E.J., Webb D.F., Woodgate B., et al., 1989. In Kundu M.R. et al. (Eds), Energetic Phenomena on the Sun, p. 77.
Solov'ev A.A., 2012. Geomagnetism and Aeronomy, vol. 52, no. 8, p. 1062.
Sterling A.C. and Moore R.L., 2005. Astrophys. J., vol. 630, p. 1148.
Su Y. and van Ballegooijen A., 2013. Astrophys. J., vol. 764, p. 91.
Svestka Z. and Cliver E.W., 1992. In Svestka Z., et al. (Eds), Proceedings of Colloquium No. 133 of IAU, Eruptive Solar Flares, Springer-Verlag Berlin Heidelberg, vol. 339, p. 1.
Uddin W., Jain R., Yoshimura K., et al., 2004. Solar Phys., vol. 225, p. 325.
van Driel-Gesztelyi L., Baker D., Torok T., et al., 2014. Astrophys. J., vol. 788, p. 85.
Vrŝnak B., 1990. Solar Phys., vol. 127, p. 129.
Webb D.F., Forbes T.G., Auras H., et al., 1994. Solar Phys., vol. 153, p. 73.
Webb D.F., Krieger A.S. and Rust D.M., 1976. Solar Phys., vol. 48, p. 159.
Williams D.R., Daker D. and van Driel-Gesztelyi L., 2013. Astrophys. J., vol. 764, p. 165.
Yardley S.L., Green L.M., Williams D.R., et al., 2016. Astrophys. J., vol. 827, p. 151.